F. Berto et alii, Frattura ed Integrità Strutturale, 38 (2016) 215-223; DOI: 10.3221/IGF-ESIS.38.29

Focussed on Multiaxial Fatigue and Fracture

Averaged strain energy density-based synthesis of crack initiation life in notched steel bars under torsional fatigue

Filippo Berto
University of Padova, Department of Management and Engineering, Vicenza (Italy)
NTNU, Department of Engineering Design and Materials, Trondheim, (Norway)
berto@gest.unipd.it

Alberto Campagnolo, Giovanni Meneghetti
University of Padova, Department of Industrial Engineering, Padova (Italy)
alberto.campagnolo@unipd.it, giovanni.meneghetti@unipd.it

Keisuke Tanaka
Meijo University, Department of Mechanical Engineering, Nagoya (Japan)
ktanaka@meijo-u.ac.jp

ABSTRACT. The torsional fatigue behaviour of circumferentially notched specimens made of austenitic stainless steel, SUS316L, and carbon steel, SGV410, characterized by different notch root radii has been recently investigated by Tanaka. In that contribution, it was observed that the total fatigue life of the austenitic stainless steel increases with increasing stress concentration factor for a given applied nominal shear stress amplitude. By using the electrical potential drop method, Tanaka observed that the crack nucleation life was reduced with increasing stress concentration, on the other hand the crack propagation life increased. The experimental fatigue results, originally expressed in terms of nominal shear stress amplitude, have been reanalysed by means of the local strain energy density (SED) averaged over a control volume having radius R_0 surrounding the notch tip. To exclude all extrinsic effects acting during the fatigue crack propagation phase, such as sliding contact and/or friction between fracture surfaces, crack initiation life has been considered in the present work. In the original paper, initiation life was defined in correspondence of a 0.1÷0.4-mm-deep crack. The control radius R_0 for fatigue strength assessment of notched components, thought of as a material property, has been estimated by imposing the constancy of the averaged SED for both smooth and cracked specimens at N_A = 2 million loading cycles.

KEYWORDS. Torsional fatigue; Notch effect; Crack initiation; Averaged SED; Electrical potential drop.

Citation: Berto, F., Campagnolo, A., Meneghetti, G., Tanaka, K., Averaged strain energy density-based synthesis of crack initiation life in notched steel bars under torsional fatigue, Frattura ed Integrità Strutturale, 38 (2016) 215-223.

Received: 14.05.2016
Accepted: 12.06.2016
Published: 01.10.2016

INTRODUCTION

Dealing with torsional and multiaxial fatigue, an anomalous phenomenon of the notch-strengthening effect was observed in circumferentially notched specimens made of austenitic stainless steels [1–3]. The fatigue life of notched specimens resulted longer than that of smooth ones, and increased with increasing stress concentration factor under the same amplitude of the nominal shear stress. This notch-strengthening effect was also observed in NiCrMo steel [4], pure titanium [5], but it was not found in carbon steels [3,6,7]. In circumferentially notched bars subjected to torsion fatigue loadings, factory-roof type fracture surfaces are obtained under low stress amplitudes and the sliding contact of the fracture surfaces causes the retardation of crack propagation [8–12]. At high stress amplitudes, instead, flat fracture surfaces are observed and the crack retardation due to sliding contact is reduced. The presence of a superimposed static tensile stress also reduces the crack surfaces contact [11].
Recently, Tanaka [13] has deeply investigated this phenomenon dealing with the fatigue behaviour of notched bars made of austenitic stainless steel, SUS316L, and carbon steel, SGV410, subjected to torsion loadings and characterized by different notch tip radii. In the present work, the experimental fatigue results have been reanalysed by means of the averaged strain energy density (SED) approach, first proposed by Lazzarin and Zambardi [14]. The crack initiation life has been considered, in such a way to exclude all extrinsic effects acting during the fatigue crack propagation phase, such as sliding contact and/or friction between fracture surfaces.

EXPERIMENTAL FATIGUE RESULTS

The materials tested in [13] were an austenitic stainless steel (SUS316L) and a carbon steel (SGV410) for structural use in nuclear power plants. The yield strength and tensile strength of SUS316L were 260 and 591 MPa, and those of SGV410 were 275 and 470 MPa.
Fig. 1 reports the geometry of the cylindrical specimens weakened by circumferential notches with three different root radii. The specimens with a notch radius ρ equal to 4.5, 1.07, and 0.22 mm are named NA, NB, and NC, respectively. The elastic stress net-section concentration factor for the shear stress under torsion for NA, NB, and NC specimens calculated by the finite element method (FEM) was 1.17, 1.55, and 2.54, respectively, while that for the tensile stress was 1.50, 2.50, and 5.07, respectively.

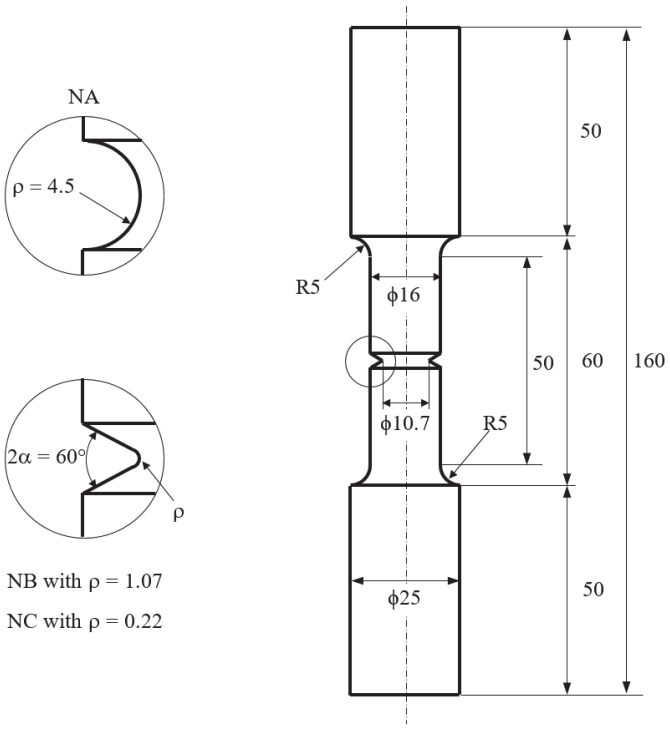

Figure 1: Geometry of the cylindrical notched specimens [13] (dimensions are in mm).

The experimental fatigue test results were obtained by adopting a nominal load ratio R equal to -1. The applied shear stress amplitude was expressed in terms of nominal stress calculated elastically from the applied torque for the minimum cross section. The fatigue tests under torsion loadings were conducted with and without superimposed static tension. In the first case, the applied static tensile stress (σ_m) equaled the applied shear stress amplitude (τ_a).
Tanaka [13] employed a DC electrical potential method to monitor the fatigue crack initiation and propagation phases. The initiation life was defined in correspondence of a 0.1÷0.4-mm-deep crack. It was observed that the total fatigue life of the austenitic stainless steel (SUS316L) increases with increasing stress concentration factor for a given applied nominal shear stress amplitude. In particular, Tanaka [13] observed that the crack nucleation life was reduced with increasing stress concentration; on the other hand the crack propagation life increased. The notch-strengthening effect has been attributed to the retarded propagation promoted by the crack surfaces contact, which occurs especially for the sharper notches. Indeed, the superposition of static tension on the fatigue torsion loading resulted in a notch-weakening behaviour, being the contact between the crack surfaces reduced. The notch strengthening effect was not observed in the SGV410 carbon steel.
On the basis of fracture surfaces and crack paths analyses [13], the difference in the notch effect on the fatigue behaviour of SUS316L and SGV410 appeared to be tied to different crack path morphologies of small cracks and three-dimensional fracture surface topographies observed by using scanning electron microscopy (SEM).
More details about the experimental results, expressed in terms of nominal shear stress amplitude, and the fracture surfaces analysis can be found in the original paper [13].

AVERAGED STRAIN ENERGY DENSITY APPROACH

The strain energy density (SED) averaged over a control volume, thought of as a material property according to Lazzarin and Zambardi [14], proved to efficiently account for notch effects both in static [14–16] and fatigue [14,17,18] structural strength problems. The idea is reminiscent of the stress averaging to perform inside a material dependent structural volume, according to the approach proposed by Neuber.
Such a method was formalized and applied first to sharp, zero radius, V-notches [14] and later extended to blunt U and V-notches [19]. When dealing with sharp V-notches, the control volume is a circular sector of radius R_0 centered at the notch tip [14]. For a blunt V-notch, instead, the volume assumes the crescent shape shown in Fig. 2 [19], where R_0 is the depth measured along the notch bisector line. The outer radius of the crescent shape is equal to $R_0 + r_0$, where r_0 depends on the notch opening angle 2α and on the notch root radius ρ according to the following expression:

$$r_0 = \frac{q-1}{q}\rho \tag{1}$$

with q defined as:

$$q = \frac{2\pi - 2\alpha}{\pi} \tag{2}$$

The control radius R_0 for fatigue strength assessment of notched components has been defined by equalling the averaged SED in two situations, i.e. the fatigue limit of un-notched and cracked specimens, respectively [4,20]. Therefore R_0 combines two material properties: the plain material fatigue limit (or the high-cycle fatigue strength of smooth specimens) and the threshold value of the SIF range for long cracks. The following expressions have been derived under plane strain hypothesis [4,20] dealing with tension (mode I) and torsion (mode III) loadings, respectively:

$$R_{0,I} = 2e_1 \cdot \left(\frac{\Delta K_{I,th}}{\Delta\sigma_0}\right)^2 = \frac{(1+\nu)(5-8\nu)}{4\pi} \cdot \left(\frac{\Delta K_{I,th}}{\Delta\sigma_0}\right)^2 \tag{3}$$

$$R_{0,III} = \frac{e_3}{1+\nu} \cdot \left(\frac{\Delta K_{III,th}}{\Delta\tau_0}\right)^2 \tag{4}$$

It should be noted that, in principle, the control radius R_0 could assume different values under mode I and mode III, so that the energy contributions related to the two different loadings should be averaged in control volumes of different size [4]. The idea of a control volume size dependent on the loading mode has been proposed for the first time in [4] dealing with the multiaxial fatigue strength assessment of notched specimens made of 39NiCrMo3 steel, then it has been successfully applied also for the fatigue strength assessment of notched components made of AISI 416 [21], cast iron EN-GJS400 [22] and titanium grade 5 alloy Ti-6Al-4V [23] subjected to combined tension and torsional loading. It is important to underline that using a Poisson's coefficient $\nu = 0.30$, Eq. (3) (being valid under plane strain hypothesis) can be re-written as follows [20,17]:

$$R_{0,I} = 0.85 \cdot \frac{1}{\pi} \cdot \left(\frac{\Delta K_{I,th}}{\Delta \sigma_0} \right)^2 \rightarrow = 0.85 \cdot a_0 \tag{5}$$

Therefore, R_0 in Fig. 2 results on the order of the El Haddad-Smith-Topper length parameter [24].

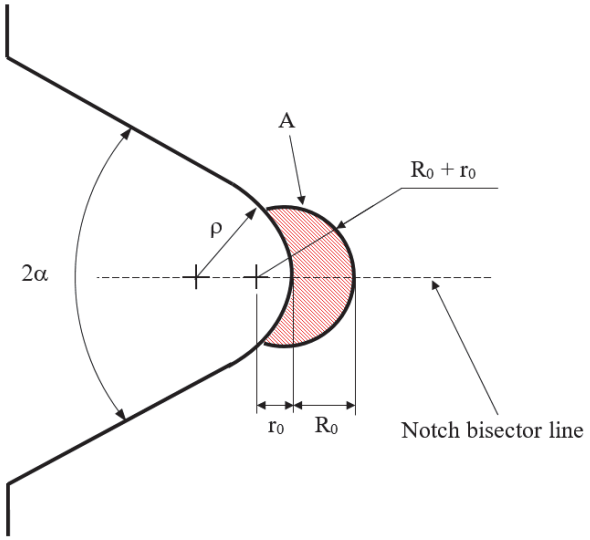

Figure 2: Control volume for specimens weakened by rounded V-notches [19].

Once the control volume is properly defined, the averaged SED can be evaluated directly from the FE results, $\Delta\overline{W}$, by summation of the strain-energies $W_{FEM,i}$ calculated for each i-th finite element belonging to the control area (A in Figs. 2-4):

$$\Delta\overline{W} = c_W \frac{\sum_A W_{FEM,i}}{A} \tag{6}$$

where the coefficient c_w accounts for the effect of the nominal load ratio R [25], when the range value of the nominal stress is applied to the FE model. It is equal to 1 for R = 0 and to 0.5 for R = −1. Equation (6) represents the so-called direct approach to calculate the averaged SED. According to a recent contribution of Lazzarin et al. [26], very coarse FE meshes can be adopted within the control volume A (see Fig. 4).

SED-BASED SYNTHESIS OF CRACK INITIATION EXPERIMENTAL DATA

The fatigue properties of the considered materials have been taken from [12,27] and are reported in Table 1. All parameters are expressed in terms of range, defined as maximum minus minimum value. The control radii $R_{0,I}$ and

$R_{0,III}$ have been calculated from Eqs. (3) and (4), respectively, where parameters e_1 and e_3 equal 0.133 and 0.414, respectively, for a Poisson's ratio $\nu = 0.3$.

Material	$\Delta\sigma_0$ (MPa)	$\Delta K_{I,th}$ (MPa $m^{0.5}$)	$R_{0,I}$ (mm)	$\Delta\tau_0$ (MPa)	$\Delta K_{III,th}$ (MPa $m^{0.5}$)	$R_{0,III}$ (mm)
SUS 316L	442	10.30	0.144	266	9.86	0.438
SGV 410	436	10.60	0.157	270	12.80	0.716

Table 1: Mechanical properties

The averaged SED values were calculated using the direct approach, $\Delta\overline{W}$, according to Eq. (6) (with about 500 finite elements inside the control volume). FE analyses have been carried out by means of Ansys® software and by adopting free mesh patterns consisting of two-dimensional, harmonic, 8-node linear quadrilateral elements (PLANE 83 of Ansys® element library), as shown in Figs. 3-4. The adopted finite element enables to analyse axis-symmetric components subjected to external loads that can be expressed according to a Fourier series expansion. Therefore, it can be employed for modelling three-dimensional axis-symmetric components under axial, bending or torsional loadings, keeping the advantage of treating two-dimensional FE analyses.

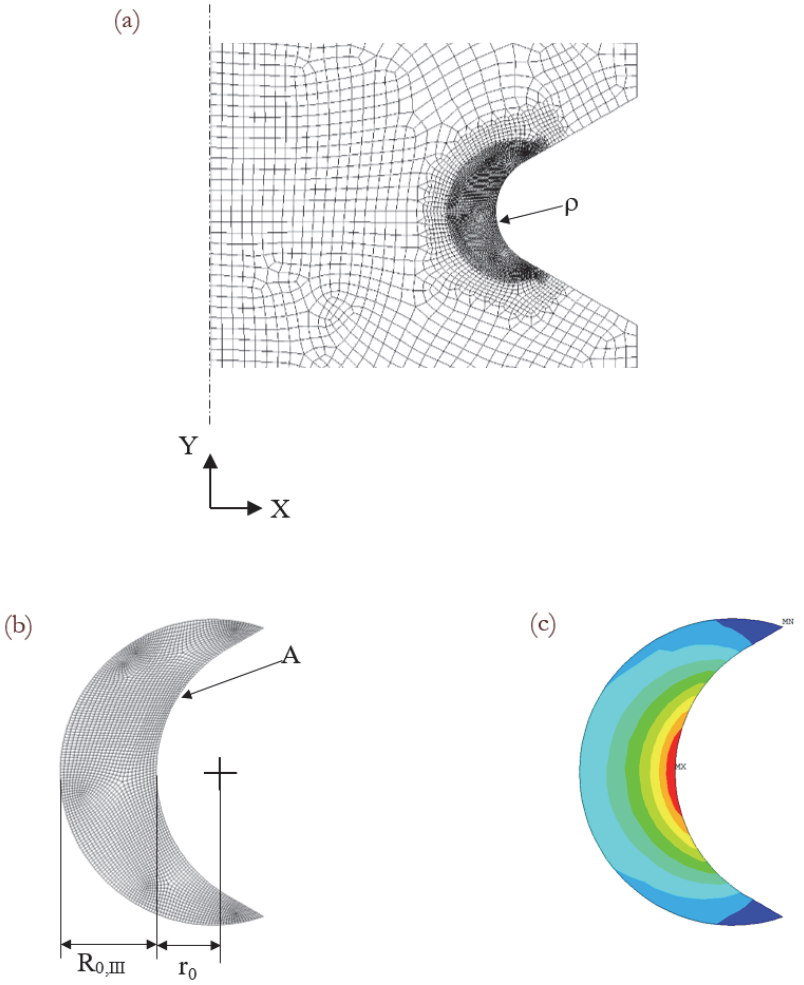

Figure 3: (a) Refined FE mesh (about 500 FE inside the control volume) adopted in the numerical analyses to evaluate the exact SED value. The Y-axis coincides with the axis of the specimen. (b) Details of the FE mesh inside the control volume and (c) SED contour lines. Considered case: NB specimen made of SGV 410 steel, with $\rho = 1.07$ mm, $R_{0,III} = 0.716$ mm, $r_0 = 0.428$ mm.

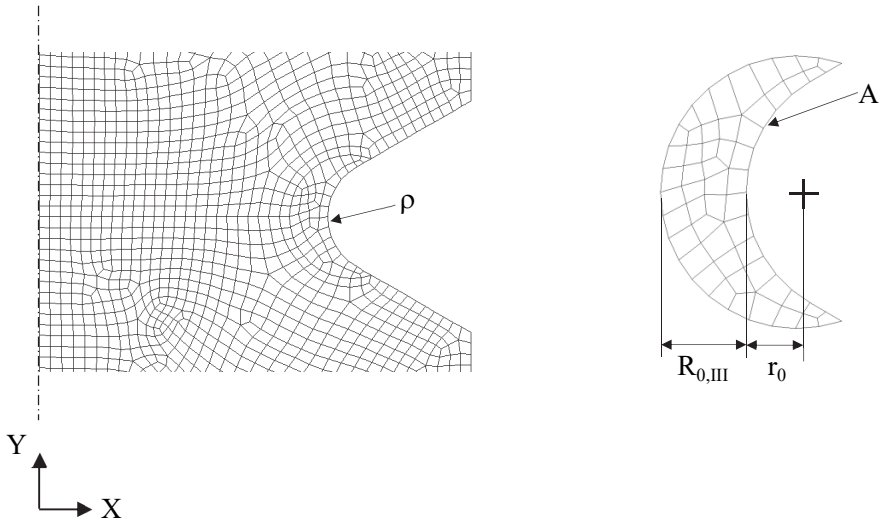

Figure 4: (a) Coarse FE mesh (about 50 FE inside the control volume) adopted in the numerical analyses producing a reduced error of 1%. The Y-axis coincides with the axis of the specimen. (b) Details of the FE mesh inside the control volume. Considered case: NB specimen made of SGV 410 steel, with ρ = 1.07 mm, $R_{0,III}$ = 0.716 mm, r_0 = 0.428 mm.

The results of the synthesis based on the local strain energy density are reported in Fig. 5. With the aim to exclude all extrinsic effects acting during the fatigue crack propagation phase, such as sliding contact and/or friction between fracture surfaces, crack initiation life, defined by Tanaka [13] in correspondence of a crack depth in the range of 0.1÷0.4 mm, has been considered in the present reanalysis. Moreover, it is important to underline that the range of the averaged strain energy density, $\Delta\overline{W}$, has been taken into account, so that the constant energy contribution of static tensile stresses has been neglected. This engineering approximation might be acceptable if crack initiation life, and not the total life, is considered, since the static tensile stress contributes more to the crack growth behaviour (i.e. sliding contact and friction between the mating surfaces) than to the crack initiation phase. The control radius $R_{0,I}$ has been calculated and reported in Table 1 only for comparison purposes.

It can be observed that in the case of SUS 316L steel, the crack initiation experimental results are well summarized in a scatter-band (Fig. 4a), characterized by an equivalent stress-based scatter index T_σ (= $\sqrt{T_w}$) equal to 1.23; this value is practically coincident with the intrinsic scatter of the original data expressed in terms of nominal stresses, which was found equal to T_σ = 1.24. However, the effects of sliding contact and/or friction between fracture surfaces during the propagation phase are evident, because the experimental results in terms of total fatigue life (see the smaller symbols: the black ones are related to pure torsion fatigue loading, while the gray ones are for torsion fatigue loading with superimposed static tension) are characterized by a high scatter, due to the difference between the fatigue lives of specimens tested with and without static tensile stress.

In the case of SGV 410 steel (Fig. 4b) the crack initiation experimental data are more scattered, T_σ being higher and equal to 1.51, while the intrinsic scatter of the original data expressed in terms of nominal stress resulted equal to T_σ = 1.17. However, in this case, the influence of extrinsic effects is almost negligible and the experimental data in terms of total fatigue life fall within the scatter-band determined using crack initiation data.

Conclusions

In the present contribution, some recent experimental fatigue test results, obtained from circumferentially notched specimens made of stainless and carbon steels, with different notch root radii and subjected to torsional fatigue loadings, have been reanalysed by means of the averaged strain energy density (SED) approach. Crack initiation life has been taken into account to exclude all extrinsic effects acting during the crack propagation phase, particularly of severely notched specimens made of stainless steel. The synthesis based on the local SED allowed to correlate fairly well the notch fatigue data for each tested material.

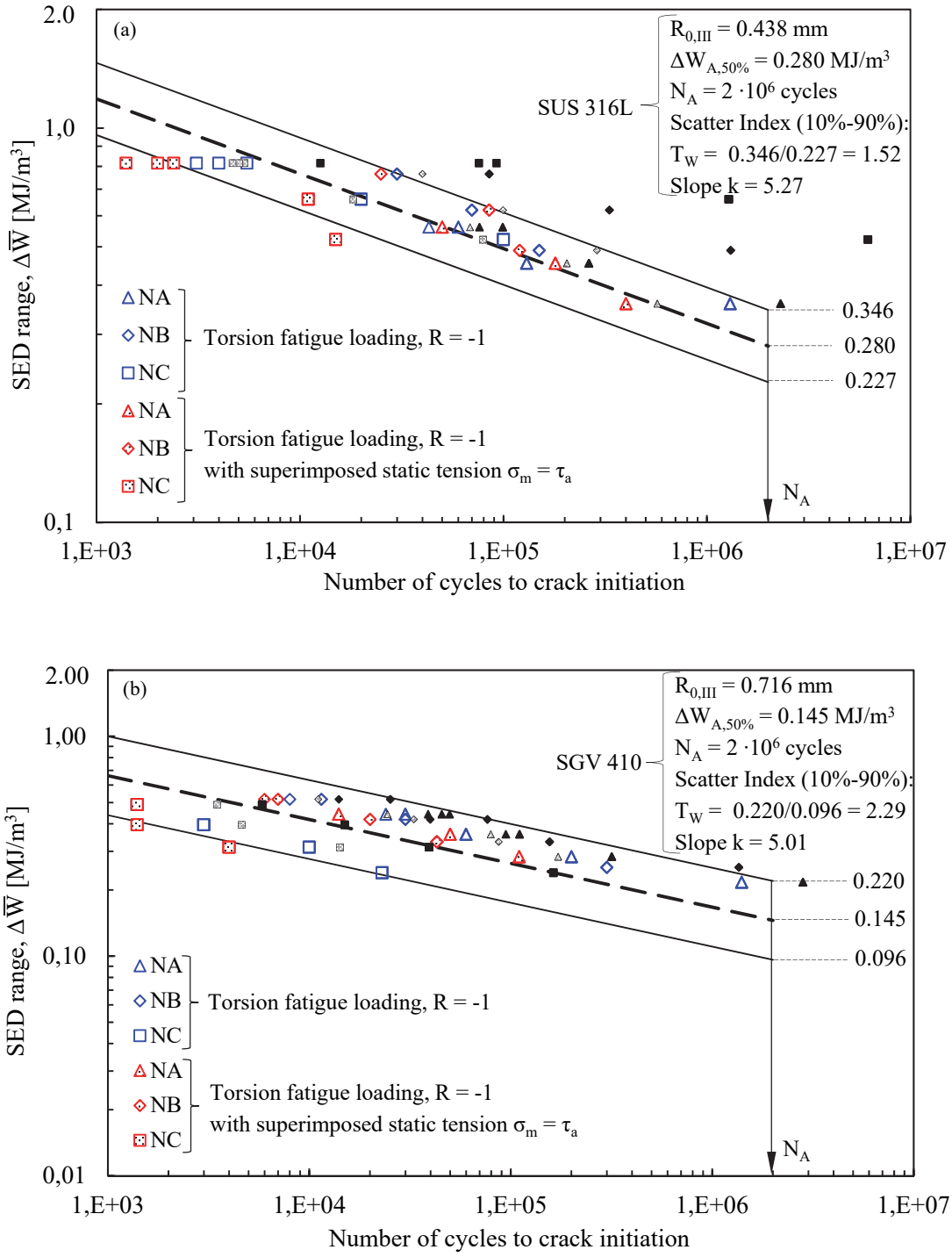

Figure 5: Averaged SED-based scatter-band calibrated on the crack initiation experimental fatigue results for (a) SUS 316L and (b) SGV 410 steels. The smaller symbols indicate the total fatigue life for comparison purposes: the black ones are for pure torsion loading, while the gray ones are for torsion loading with superimposed static tension.

REFERENCES

[1] Tanaka, K., Hashimoto, A., Narita, J., Egami, N., Fatigue life of circumferentially notched bars of austenitic stainless

steel under cyclic torsion with and without static tension, J Soc Mater Sci., 58 (2009) 1044–1050.
[2] Tanaka, K., Small fatigue crack propagation in notched components under combined torsional and axial loading, Procedia Eng., 2 (2010) 27–46. doi:10.1016/j.proeng.2010.03.004.
[3] Ohkawa, C., Ohkawa, I., Notch effect on torsional fatigue of austenitic stainless steel: Comparison with low carbon steel, Eng. Fract. Mech., 78 (2011) 1577–1589. doi:10.1016/j.engfracmech.2011.01.015.
[4] Berto, F., Lazzarin, P., Yates, J.R., Multiaxial fatigue of V-notched steel specimens: A non-conventional application of the local energy method, Fatigue Fract. Eng. Mater. Struct., 34 (2011) 921–943. doi:10.1111/j.1460-2695.2011.01585.x.
[5] Okano, T., Hisamatsu, N., Effect of notch of torsional fatigue property of pure titanium, Proc. 31 Symp. Fatigue, Soc. Mater. Sci. Japan., 31 (2012) 129–133.
[6] Atzori, B., Berto, F., Lazzarin, P., Quaresimin, M., Multi-axial fatigue behaviour of a severely notched carbon steel, Int. J. Fatigue, 28 (2006) 485–493. doi:10.1016/j.ijfatigue.2005.05.010.
[7] Tanaka, K., Ishikawa, T., Narita, J., Egami, N., Fatigue life of circumferentially notched bars of carbon steel under cyclic torsion with and without static tension, J Soc Mater Sci. 60 (2011).
[8] Ritchie, R.O., McClintock, F.A., Nayeb-Hashemi, H., Ritter, M.A., Mode III fatigue crack propagation in low alloy steel, Metall. Trans. A., 13 (1982) 101–110. doi:10.1007/BF02642420.
[9] Tschegg, E.K., A contribution to mode III fatigue crack propagation, Mater. Sci. Eng. 54 (1982) 127–136. doi:10.1016/0025-5416(82)90037-4.
[10] Tschegg, E.K., The influence of the static I load mode and R ratio on mode III fatigue crack growth behaviour in mild steel, Mater. Sci. Eng., 59 (1983) 127–137. doi:10.1016/0025-5416(83)90094-0.
[11] Tanaka, K., Akiniwa, Y., Nakamura, H., J-integral approach to mode III fatigue crack propagation in steel under torsional loading, Fatigue Fract. Eng. Mater. Struct., 19 (1996) 571–579. doi:10.1111/j.1460-2695.1996.tb00993.x.
[12] Yu, H., Tanaka, K., Akiniwa, Y., Estimation of torsional fatigue strength of medium carbon steel bars with a circumferential crack by the cyclic resistance-curve method, Fatigue Fract. Eng. Mater. Struct., 21 (1998) 1067–1076. doi:10.1046/j.1460-2695.1998.00105.x.
[13] Tanaka, K., Crack initiation and propagation in torsional fatigue of circumferentially notched steel bars, Int. J. Fatigue, 58 (2014) 114–125. doi:10.1016/j.ijfatigue.2013.01.002.
[14] Lazzarin, P., Zambardi, R., A finite-volume-energy based approach to predict the static and fatigue behavior of components with sharp V-shaped notches, Int. J. Fract., 112 (2001) 275–298. doi:10.1023/A:1013595930617.
[15] Berto, F., Lazzarin, P., Recent developments in brittle and quasi-brittle failure assessment of engineering materials by means of local approaches, Mater. Sci. Eng. R Reports, 75 (2014) 1–48. doi:10.1016/j.mser.2013.11.001.
[16] Campagnolo, A., Berto, F., Leguillon, D., Fracture assessment of sharp V-notched components under Mode II loading: a comparison among some recent criteria, Theor. Appl. Fract. Mech., (2016) in press. doi:10.1016/j.tafmec.2016.02.001.
[17] Livieri, P., Lazzarin, P., Fatigue strength of steel and aluminium welded joints based on generalised stress intensity factors and local strain energy values, Int. J. Fract., 133 (2005) 247–276. doi:10.1007/s10704-005-4043-3.
[18] Berto, F., Campagnolo, A., Chebat, F., Cincera, M., Santini, M., Fatigue strength of steel rollers with failure occurring at the weld root based on the local strain energy values: modelling and fatigue assessment, Int. J. Fatigue, 82 (2016) 643–657. doi:10.1016/j.ijfatigue.2015.09.023.
[19] Lazzarin, P., Berto, F., Some expressions for the strain energy in a finite volume surrounding the root of blunt V-notches, Int. J. Fract., 135 (2005) 161–185. doi:10.1007/s10704-005-3943-6.
[20] Lazzarin, P., Berto, F., From Neuber's Elementary Volume to Kitagawa and Atzori's Diagrams: An Interpretation Based on Local Energy, Int. J. Fract., 135 (2005) L33–L38. doi:10.1007/s10704-005-4393-x.
[21] Berto, F., Lazzarin, P., Fatigue strength of structural components under multi-axial loading in terms of local energy density averaged on a control volume, Int. J. Fatigue, 33 (2011) 1055–1065. doi:10.1016/j.ijfatigue.2010.11.019.
[22] Berto, F., Lazzarin, P., Tovo, R., Multiaxial fatigue strength of severely notched cast iron specimens, Int. J. Fatigue, 67 (2014) 15–27. doi:10.1016/j.ijfatigue.2014.01.013.
[23] Berto, F., Campagnolo, A., Lazzarin, P., Fatigue strength of severely notched specimens made of Ti-6Al-4V under multiaxial loading, Fatigue Fract. Eng. Mater. Struct., 38 (2015) 503–517.
[24] El Haddad, M.H., Topper, T.H., Smith, K.N., Prediction of non propagating cracks, Eng. Fract. Mech., 11 (1979) 573–584. doi:10.1016/0013-7944(79)90081-X.
[25] Lazzarin, P., Sonsino, C.M., Zambardi, R., A notch stress intensity approach to assess the multiaxial fatigue strength of welded tube-to-flange joints subjected to combined loadings, Fatigue Fract. Eng. Mater. Struct., 27 (2004) 127–140. doi:10.1111/j.1460-2695.2004.00733.x.
[26] Lazzarin, P., Berto, F., Zappalorto, M., Rapid calculations of notch stress intensity factors based on averaged strain energy density from coarse meshes: Theoretical bases and applications, Int. J. Fatigue, 32 (2010) 1559–1567.

doi:10.1016/j.ijfatigue.2010.02.017.
[27] Tanaka, K., Akiniwa, Y., Yu, H., The propagation of a circumferential fatigue crack in medium-carbon steel bars under combined torsional and axial loadings. In: Mixed-Mode Crack Behaviou, in: K. Miller, D. McDowell (Eds.), Mix. Crack Behav. ASTM 1359, West Conshohocked, PA, (1999) 295–311.